High temperature properties of the Cr-Nb-Al-N coatings with increasing Al contents

W.Z. Li, T. Polcar, M. Evaristo, A. Cavaleiro

PII: S0257-8972(13)00371-X
DOI: doi: 10.1016/j.surfcoat.2013.04.027
Reference: SCT 18495

To appear in: *Surface & Coatings Technology*

Received date: 20 December 2012
Accepted date: 11 April 2013

Please cite this article as: W.Z. Li, T. Polcar, M. Evaristo, A. Cavaleiro, High temperature properties of the Cr-Nb-Al-N coatings with increasing Al contents, *Surface & Coatings Technology* (2013), doi: 10.1016/j.surfcoat.2013.04.027

High temperature properties of the Cr-Nb-Al-N coatings with increasing Al contents

W.Z. Li [a, b,*], T. Polcar [c,d], M. Evaristo [a], A. Cavaleiro [a,*]

[a] SEG-CEMUC - Department of Mechanical Engineering, University of Coimbra, Rua Luís Reis Santos, P-3030 788 Coimbra, Portugal

[b] School of Materials Science and Engineering, Guangxi University, Nanning 530004, PR China

[c] National Centre for Advanced Tribology at Southampton (nCATS), School of Engineering Sciences, University of Southampton, Highfield, Southampton, SO17 1BJ, Hampshire, UK

[d] Department of Control Engineering, Faculty of Electrical Engineering, Czech Technical University in Prague, Technická 2, Prague 6, Czech Republic

Corresponding author. Tel.: +351 239 790 745; fax: +351 239 790 701.

E-mail address: albano.cavaleiro@dem.uc.pt (A. Cavaleiro), wz-li@hotmail.com (W.Z. Li).

Abstract

Cr-Nb-Al-N coatings with Al content from 0 to 12 at.% were deposited by d.c. reactive magnetron sputtering. The coatings were annealed in protective atmosphere at 800 and 900 ^{o}C for 1h and exposed to air at 800, 900 and 1200 ^{o}C for different times. The chemical composition, structure, microstructure, hardness and adhesive/cohesive strength of the coatings, in as-deposited and annealed conditions, were investigated and the oxidation resistance was evaluated. As expected, the Al content increased gradually in the coating with increasing power density in Al target; nitrogen was kept approximately constant. All coatings exhibited columnar cross section morphology and fcc NaCl-type B1 phase structure. After thermal annealing, an increase in the

grain size and a decrease in the lattice parameter were observed, which led to either a decrease in the hardness or lower adhesion/cohesion strength than the as-deposited coatings. The onset oxidation temperature was approx. 900 ^{o}C for all coatings. High Al content coatings showed minimum oxidation when exposed to 800 ^{o}C for 2h and to 900 ^{o}C for 0.5h in air. The Al-free and low Al coatings exhibited lower oxidation resistance; Cr_2O_3 and $CrNbO_4$ coexisting together although signs of the cubic nitride phase were still detected. The increase of Al was beneficial to the improvement of the thermal stability and oxidation resistance of the Cr-Nb-Al-N coatings.

Keywords: Cr-Nb-Al-N coatings; mechanical properties; thermal stability; oxidation resistance; high temperature

1. Introduction

Recently, machining technology has been developed towards high precision, high speed, high efficiency and low emission, which has required cutting tools with higher hardness, lower wear-resistance, and higher thermal stability and oxidation resistance [1]. Due to suitable hardness, low friction coefficient and strong adhesion to metal substrates, Cr-N coatings have been widely used on cutting tools for several decades [2]. However, those increasing requirements are making binary Cr-based nitride coatings inadequate in many applications [2-4].

Alloying is an effective method to improve the properties of Cr-based coating. By using alloy elements, especially those with large atomic radius, e.g. Zr, Nb, Ta and W [5-8], ternary nitride coatings exhibit higher hardness and improved high temperature properties than the binary system. Furthermore, it was reported that NbN with high melting point, good mechanical properties and excellent corrosion resistance have also been used in many fields as protecting coatings [9-12]. Therefore, Cr-N coatings with Nb alloying were considered appropriate for the protection of

cutting tools. However, Hsieh et al. [13] found that Cr-Nb-N coatings started to oxidize just over 500 ^{o}C independently of the Nb/Cr ratio and their wear rate was rather high even at the room temperature.

The addition of Al has often been reported to improve the mechanical properties and thermal stability of Cr-based and Ti-based nitride coatings [2, 14]. Due to age hardening effect, the coating hardness can be enhanced ~30 % after thermal annealing [15, 16], and the onset oxidation temperature was increased about 100~200 ^{o}C with the introduction of Al into the coatings [17, 18]. Moreover, Barshilia et al [19] found that the addition of Al could also improve the thermal stability and oxidation resistance of Nb-based nitride coatings. Although Franz et al. [20] showed that the onset oxidation temperature markedly increased with the Al content in the Nb-based nitride coatings, they suggested that the mechanical properties would be weakened as high Al content was added. Thus, the influence of Al on the high temperature properties of these nitride coatings is still not understood. Till now research of the effects of Al on the properties of the Cr-Nb-based quarternary nitride coatings has not yet been reported. The thermal stability and oxidation resistance of such quarternary coatings are still unclear.

In this paper, Cr-Nb-Al-N coatings with different Al contents were deposited by d.c. reactive magnetron sputtering technology. The influence of Al on the structure and mechanical properties of the coatings before and after thermal annealing was investigated, and the oxidation resistance of the coatings was studied.

2. Experimental procedure

Cr-Nb-(Al-)N coatings were deposited by d.c. reactive magnetron sputtering in unbalanced mode. The configuration of the deposition chamber can be found in a previous paper [21].

Polished M2 (AISI) steel coupons (for mechanical properties measurement), Fecralloy (for oxidation test; chemical composition $Fe_{72.8}Cr_{22}Al_5Y_{0.1}Zr_{0.1}$), polycrystalline alumina slices (for TGA analysis) and (111) silicon wafers (for chemical composition and thickness measurements, and microstructural observation) were used as substrate materials. Before loading into the chamber, the substrates were ultrasonically cleaned in acetone and alcohol each for 15 min, respectively. After the chamber was evacuated to less than 1.5×10^{-4} Pa, an Ar+ ion sputter-etching was carried out for 20 min with a negative substrate bias of 400 V to remove the surface contamination. In order to enhance the coating's adhesion, a ~200 nm thick Cr interlayer was first deposited in Ar atmosphere. The Cr-Nb-(Al-)N coatings were deposited at -70 V bias under a mixed gas flow of Ar 35 sccm and N_2 48 sccm. During deposition, the power densities for pure Nb and pure Cr targets were fixed as 1.5 W/cm^2 and 2.25 W/cm^2 respectively, and the Al target's power density was set as 0, 0.75, 1.5, 2.25 and 3.0 W/cm^2, respectively. The deposition time was 150 min.

The samples were annealed at 800 and 900 ^{o}C for 1 h in Ar + 5% H_2 atmosphere. Thermogravimetric analyses (TGA) were performed by exposing the samples to industrial air (99.995% purity) in a thermogravimetric analysis equipment (Setsys evolution 1750). The maximum temperature was set to 1200 ^{o}C with a heating rate of 10 ºC/min to determine the coating onset oxidation temperature, and afterwards kept the samples at 1200 ^{o}C for 1h. High temperature oxidation-resistance tests were conducted at 800 ^{o}C for 2 h and 900 ^{o}C for 0.5 h, respectively. The former was performed in the TGA equipment with a heating rate 30 ºC/min. The latter was done by inserting the samples in alumina crucibles placed in a 900 ^{o}C tube furnace, and subsequently cooling down to room temperature.

The thickness of the coatings was measured by profilometry. The chemical composition of the

coating was determined by Cameca SX-50 Electron Probe Microanalysis (EPMA). The crystal structure of the coatings was analysed by X-ray diffraction (XRD) with Co Kα radiation (λ = 0.178897 nm) in grazing mode (2°). The hardness (H) and Young's modulus (E) of the coatings were measured using a nanoindenter (Micro Materials NanoTest) with a diamond Berkovich tip under 10 mN applied load. 12 measurements were conducted for each sample and the results were analysed using the Oliver and Pharr method [22]. The adhesion/cohesion of the coatings to M2 steel substrate was evaluated by scratch testing. The load was increased linearly from 0 N to 80 N using a Rockwell C indenter with a 200 μm tip radius. The loading speed was 100 N/min and the scratch speed was 10 mm/min.

3. Results and discussion

3.1 Chemical composition and microstructure

Table 1 shows that Al content increases gradually from 0 to 12 at.% with the increase of Al target power density. Simultaneously a slow decrease in Nb and Cr contents is observed, although N content remains almost constant (slightly above 50 at.%). The coating thickness increased from 1.70 μm to 2.05 μm with increasing Al target power density from 0 up to 3.0 W/cm^2. For simplicity, a designated name is assigned to each coating sample according to its chemical composition, as shown in Table 1.

Figure 1 shows the surface topography analysed by AFM and the cross-sectional SEM morphology of the as-deposited coatings. The coating thickness increases with Al content, in good agreement with the results from profilometry shown in Table 1. SEM images reveal columnar structures in all coatings (Fig.1 (d-f)). The dimension of the columns decreases with increasing Al content, as confirmed by the decrease in the surface features dimensions in AFM observations,

which decreased from 250 nm. for Al-free coating (Fig.1 a), down to ~150 nm for CrNb8Al10N coating (Fig.1 c). Coatings with smaller grain size are often suggested to have stronger oxidation resistance due to an improved elemental diffusion to form protective surface scales [23]. From AFM images, it is also observed that the coatings are quite smooth, especially for CrNb9Al4N sample, with average surface roughness in the range from 7.8 nm up to 11.7 nm (Fig.1 (a-c)).

XRD results show that structurally all coatings have the fcc B1 (NaCl type) nitride phase (Fig. 2a). Generally, the diffraction peaks are closer to the peaks of pure cubic CrN phase (ICDD 11-0065, a_o=4.14 Å) than to the cubic NbN phase (ICDD 38-1155, a_o=4.39 Å) suggesting a mixed (Cr, Nb)N phase with lattice parameter in between those of pure compounds. The higher amount of Cr in relation to Nb places the peaks position closer to CrN phase. With the addition of Al, no significant changes in the peaks positions could be detected. Cubic AlN phase has lattice parameters close to CrN (c-AlN: ICDD 25-1495, a_o=4.12 Å) and, therefore, substitution of Cr with Al will not significantly influence the peaks position (Cr content decreases with increasing Al content). Mayrhofer et al [24] also found only a small decrease (from 4.155 to 4.153 Å) in lattice parameter values of $Cr_{1-x}Al_xN$ for x=0.21, value close to the maximum Al content added to Cr-Nb-N coatings in this work. Wurtzite AlN phase (w-AlN: ICDD 25-1133, a_o=b_o=3.11 Å, c_o=4.98 Å) has not been detected. The lattice parameters calculated from (111) diffraction peak are shown in Fig. 2(b) and confirm the above discussion in relation to peaks position. The lattice parameter is in-between that of cubic CrN (a_o=4.14 Å) and cubic NbN (a_o=4.39 Å) and with increasing Al contents no significant changes in lattice parameters can be detected. Fig. 2(b) shows that the coatings grain size calculated by Scherrer's equation from the (111) peak is in the range from 8 to 10 nm. The small decrease in the grain size when Al is added content indicates

that Al can cause grain size refining.

3.2 Thermal stability

To investigate thermal stability, as-deposited coatings were annealed in protective atmosphere at 800 ^{o}C and 900 ^{o}C for 1h. Fig.3 shows the XRD patterns, grain size and lattice parameter of the coatings after thermal annealing. No significant differences in the XRD results were found for the same coating annealed at 800 ^{o}C or 900 ^{o}C (Fig. 3a). Cr_2N and/or w-AlN phases, which were often reported as the results of the CrN-based phase transformation during thermal annealing above 700 ^{o}C when multi-elemental nitride coatings are deposited by vacuum arc technology [25, 26], were not detected in the annealed coatings. Compared to as-deposited coatings, peaks positions for the annealed coatings are closer to the standard one of cubic CrN phase. Additionally, several weak peaks are detected on Al-free coatings (Fig. 3(a)), which should be attributed to the formation of oxide phases resulting from residual oxygen in the furnace atmosphere. In Fig. 3(b), calculated lattice parameter experiences a marked decrease after thermal annealing with increasing Al content. The lattice parameter is about 4.19 Å for the Al-free coating and is reduced to 4.14 Å for the highest Al-content coating, which is equal to the value of cubic CrN phase. From Fig. 3(b), it is found that the grain size is slightly larger than that in the as-deposited coatings. For example, the grain size for the as-deposited, 800 ^{o}C and 900 ^{o}C annealed CrNb8Al10N coating is 8.3 nm, 9.1 nm and 9.4 nm, respectively. The grain size of annealed coatings is almost independent of aluminum content. We can summarize that the cubic Cr(Nb)N and Cr(Nb, Al)N phases are thermally stable up to 900 ^{o}C.

3.3 Mechanical properties

The hardness and Young's modulus of the as-deposited and 900 ^{o}C annealed coatings are shown

in Fig.4. The trends for the hardness or Young's modulus with the Al content are similar in the as-deposited and annealed coatings. With the addition of Al, the hardness increases, being kept approximately constant thereafter as a consequence of the combined effects of solid solution hardening, lattice distortion and grain size refinement promoted by Al atoms in the nitride lattice. On the other hand, Young's modulus exhibits a monotonical increase with the Al content in the coatings which should be related with the stronger covalent nature of Al-N bonding [27]. After annealing, the hardness is expected to decrease compared to the as-deposited state, due to grain growth, possible reduction of lattice distortion [2], decrease of residual stress and presence of softer oxide phases.

Strong adhesion strength of a coating onto a substrate is always required before the coating is put into application. For thin hard coatings, scratch testing is the most common method to evaluate the adhesion/cohesion strength [21, 28]. In the present research, Cr-Nb-(Al-)N coatings were scratched by a diamond indenter before and after thermal annealing, and the critical load of substrate exposure (*L*c3) is summarized in Table 1. After scratch testing, the tracks were observed by optical microscopy. From Fig. 5, it is obvious that the track morphologies for the as-deposited coatings are very different from those of the annealed ones. No evident substrate exposure (*L*c3) is found in the as-deposited coatings (Fig. 5(a, c, e)). Only small area edge chipping (*L*c2) is detected at ~46 N on the low Al coating (Fig. 5(c)). Such edge chipping is often observed on hard coating samples deposited on medium hardness steel substrates [21, 29]. For the annealed coatings, the substrate exposure was found in all samples (Fig. 5(b, d, f)). *L*c3 increases from 29 N to 49 N when the Al content is raised up to 9.6 at%. The lower *L*c3 value in the annealed Al-free coating can be attributed to the presence of oxides on the coating surface as confirmed by XRD

measurements. Substrate exposure is due to the widening and deepening of the scratch track in the annealed sample compared to the as-deposited counterpart. Due to the softening of steel substrate after thermal annealing [30], the higher plastic deformation of the substrate will induce a higher stress state in both the coating and the interface, leading to a premature failure of the coated sample. Such a fact combined with the coating softening induced during thermal annealing, the residual stress release and the presence of oxide layers, give rise to lower critical loads in relation to as-deposited samples even though the interface between the coating and the substrate may be strengthened due to elemental interdiffusion during thermal annealing.

3.4 Oxidation resistance

The onset oxidation temperature is very important for predicting the high temperature behavior of a hard coating system. Thermogravimetry performed with slow heating rate is an effective method to determine the onset oxidation temperature. Fig. 6(a) shows the curves of mass gain vs. temperature of the Al-free, CrNb9Al4N and CrNb8Al10N coatings till 1200 ^{o}C. The curves in this figure clearly show a decrease of the mass gain with the addition of Al, although the onset oxidation temperature is confounded to be similar about 900 ^{o}C for all the studied samples. Lin et al also reported that the addition of Al can improve the oxidation resistance and thermal stability of Cr-N coatings [17]. They found that the onset temperature for CrN_x coating was 600 ^{o}C rising to 650 ^{o}C for $Cr_{0.77}Al_{0.23}N$ coating, and 700 ^{o}C for $Cr_{0.40}Al_{0.60}N$ coating. In the present research, the fairly higher onset oxidation temperature, about 150 ^{o}C, should be attributed to the presence of Nb, whereas the presence of Al improves the coating oxidation resistance.

XRD patterns of the 1h exposed coatings at 1200 ^{o}C are shown in Fig. 6(b). From XRD results, Cr_2O_3 is found to be the main oxidation product, although high amount of $CrNbO_4$ phase (reaction

product of Cr_2O_3 and Nb_2O_5 [31]) was also detected. Al_2O_3 peaks were observed in the high Al coating CrNb8Al10N. From the cross-sectional SEM images (not shown), homogenously porous oxides were found adhered to the Al_2O_3 substrate in the Al-free coating; in other words, the Al-free coating was fully oxidized. For the high Al coating, in addition to dense oxide layer, nitride layer was still detected distinctly close to the substrate. Denser Al_2O_3 or Cr_2O_3 scales can act as an effective diffusion barrier to limit the inward diffusion of ions and protect the underneath coating from oxidation attack [32, 33].

To further investigate the oxidation resistance, the coating samples were exposed to 800 ^oC for 2h. The TGA curves, XRD patterns and surface SEM images are shown in Fig. 7. Fig. 7(a) shows that three coatings exhibit parabolic mass gains vs. exposure time; the Al-containing coatings show a much slower mass gain than the Al free coating. After 2h exposure, the mass gain is double in Al-free coating in relation to the high Al coating. XRD patterns show mainly Cr_2O_3 and $CrNbO_4$ in Al-free coating, although low intensity peaks of the original cubic nitride phases are still detected. The situation is inversed for the low Al coating for which nitride peaks are predominant. This trend reaches its extreme, when only the cubic nitride phase diffraction peaks are detected in high Al coating; the diffraction peaks are a slightly narrower than those of the protective 800 ^oC annealed film. The grain size calculated from Scherrer's equation is ~10.5 nm, indicating that prolonging the exposure time may contribute the grain growth.

Fig. 7(c) shows that Al-free coating surface is almost covered by particles with different sizes. EDS indicates that the particles are mixed-oxides of Nb and Cr (Nb 23.6 at.%, Cr 14.9 at.% and O 61.5 at.%). On low Al coating surface, some large oxides particles are scattered (Fig. 7(d)). Hardly any oxide particles are found on the CrNb8Al10N coating (Fig. 7 (e)). The formation of cracks on

the high Al coating should result from the residual stress release during cooling down from high exposure temperature.

It is evident from the sample mass gain vs. exposure time shown in Fig. 6(a) that the high Al coating starts to oxidize at about 900 ^{o}C. Therefore, the selected coatings were annealed in air at 900 ^{o}C for 0.5 h. Fig. 8 presents the XRD patterns and surface SEM micrographs of the exposed coatings. Compared to the 800 ^{o}C/2h annealed samples, similar XRD diffraction peaks of oxides phases are detected on the Al-free and low Al coatings (Fig. 8(a)). CrNb8Al10N coating shows only the nitride phase with a grain size of ~11.8 nm, i.e. slightly larger than that of the sample annealed in protective atmosphere at the same temperature. SEM shows similar oxide particles covering entire Al-free coating surface (Fig. 8(b)), whereas Al-containing coatings exhibit smooth surface with only small number of oxide particles (Fig. 8(c, d)). As before, the cracks are clearly visible on the surface of the highest Al coating sample (Fig. 8(d)); much smaller cracks were observed as well in CrNb10Al4N sample. The oxidation analysis demonstrates that increase in Al content significantly improves oxidation resistance of Cr-Nb-Al-N coatings. On the other hand, the cracks observed on the surface of Al-containing coatings could results in detachment of the protective oxide layer, particularly during sliding at high temperature.

4. Conclusion

Cr-Nb-Al-N coatings were deposited by d.c. reactive magnetron sputtering technique. The Al content in the coating increased from 0 to 12 at.% as Al target power density was increased from 0 to 3 W/cm^2 with a step of 0.75 W/cm^2 during deposition. The coatings exhibited columnar structure with average surface roughness of about 8~12 nm. Only the fcc B1 (NaCl type) nitride phase was detected in all coatings.

After thermal annealing at 800 and 900 ^{o}C in protective atmosphere, no phase transformation was detected in the coatings and the grain size increased by 1~2 nm. The decrease in the hardness was due to grain growth, reduced lattice distortion and residual surface oxidation. The softening of substrate and coating, and the formation of thin oxides on the Al-free coating led to a decline in the adhesion/cohesion strength of the annealed coatings.

The onset oxidation temperature was close to 900 ^{o}C for all coatings. After thermal exposure at 800 ^{o}C for 2h and 900 ^{o}C for 0.5h, mainly Cr_2O_3 and $CrNbO_4$ were formed. The cubic nitride phase remained on Al-free and low Al coatings. Hardly any oxidation took place on the high Al coating. The Al-containing coatings exhibited strong thermal stability and oxidation resistance, and the coating oxidation resistance was improved with the increase of Al content in the coating.

Acknowledgements

This work was supported by the Portuguese Foundation for Science and Technology (FCT, SFRH/BPD/76925/2011), the National Natural Science Foundation of China (Grant No.51001032) , the Ministry of Education of the Czech Republic (project MSM 6840770038) and Guangxi Science Foundation (Grant No. 0731013), which is gratefully acknowledged. The authors are grateful to João Carlos for EPMA analysis, Ricardo Serra for AFM observation, and Jorge Corker for TGA measurement and Nelson Duarte for XRD analyses.

References

[1] W. Kalss, A. Reiter, V. Derflinger, C. Gey, J.L. Endrino, Int. J. Refract. Met. H. 24 (2006) 399.

[2] P.H. Mayrhofer, C. Mitterer, L. Hultman, H. Clemens, Prog. Mater. Sci. 51 (2006) 1032.

[3] Z.G. Zhang, O. Rapaud, N. Bonasso, D. Mercs, C. Dong, C. Coddet, Vacuum 82 (2008) 1332.

[4] T. Polcar, R. Martinez, T. Vítů, L. Kopecký, R. Rodriguez, A. Cavaleiro, Surf. Coat. Technol. 203 (2009) 3254.

[5] S.M. Kim, B.S. Kim, G.S. Kim, S.Y. Lee, B.Y. Lee, Surf. Coat. Technol. 202 (2008) 5521.

[6] J.N. Tan , J.H. Hsieh, Surf. Coat. Technol. 167 (2003) 154.

[7] P. Hones, R. Consiglio, N. Randall, F. Leacutevy, Surf. Coat. Technol. 125 (2000) 179.

[8] Y. I. Chen, Y.T. Lin, L.C. Chang, J.W. Lee, Surf. Coat. Technol. 206 (2011) 1640.

[9] M. Benkahoul, E. Martinez, A. Karimi, R. Sanjinés, F. Lévy, Surf. Coat. Technol. 180-181 (2004) 178.

[10] G.A. Fontalvo, V. Terziysk, C. Mitterer, Surf. Coat. Technol. 202 (2007) 1017.

[11] M. Fenker, M. Balzer, R.V. Büchi, H.A. Jehn, H. Kappl, J.J. Lee, Surf. Coat. Technol. 163-164 (2003) 169.

[12] D.B. Lewis, D. Reitz, C. Wüstefeld, R. Ohser-Wiedemann, H. Oettel, A.P. Ehiasarian, P.Eh. Hovsepian, Thin Solid Films 503 (2006) 133.

[13] J.H. Hsieh, C. Li, A.L.K. Tan, C.K. Poh, N.J. Tan, Surf. Coat. Technol. 177-178 (2004) 299.

[14] A. Hörling, L. Hultman, M. Odén, J. Sjölén, L. Karlsson, Surf. Coat. Technol. 191 (2005) 384.

[15] P.H. Mayrhofer, A. Hörling , L. Karlsson, J. Sjoölén, T. Larsson, C. Mitterer, L. Hultman, Appl. Phys. Lett. 83 (2003) 2049.

[16] R. Rachbauer, S. Massl, E. Stergar, D. Holec, D. Kiener, J. Keckes, J. Patscheider, M. Stiefel, H. Leitner, P. H. Mayrhofer, J. Appl. Phys. 110 (2011) 023515.

[17] J. Lin, B. Mishra, J.J. Moore, W.D. Sproul, Surf. Coat. Technol. 202 (2008) 3272.

[18] L. Chen, J. Paulitsch, Y. Du, P. H. Mayrhofer, Surf. Coat. Technol. 206 (2012) 2954.

[19] H.C. Barshilia, B. Deepthi, K.S. Rajam, K.P. Bhatti, S. Chaudhary, J. Mater. Res. 23 (2008) 1258.

[20] R. Franz, M. Lechthaler, C. Polzer, C. Mitterer, Surf. Coat. Technol. 204 (2010) 2447.

[21] W.Z. Li, M. Evaristo, A. Cavaleiro, Surf. Coat. Technol. 206 (2012) 3764.

[22] W.C. Oliver, G.M. Pharr, J. Mater. Res. 7 (1992) 1564.

[23] F. H. Wang, Oxid. Met. 48 (1997) 215.

[24] P.H. Mayrhofer, H. Willmann, A.E. Reiter, Surf. Coat. Technol. 202 (2008) 4935.

[25] S. Zhang, L. Wang, Q. Wang, M. Li, Surf. Coat. Technol. 214 (2013) 153..

[26] T. Polcar, A. Cavaleiro, Mater. Chem. Phys. 129 (2011) 195.

[27] K. Polychronopoulou, N.G. Demas, C. Rebholz, A.A. Polycarpou, Tribol. Lett. 32 (2008) 117.

[28] J. Lin, J.J. Moore, W.D. Sproul, B. Mishra, Z. Wu, J. Wang, Surf. Coat. Technol. 204 (2010) 2230.

[29] J. Stallard, S. Poulat, D.G. Teer, Tribol. Int. 39 (2006) 159.

[30] A. Cavaleiro, A.P. Marques, J.V. Fernandes, N.J.M. Carvalho, J.Th. De Hosson, J. Mater. Res. 20 (2005) 1356.

[31] B.I. Portillio, S.K. Varma, Metall. Mater.Trans. A, 43 (2012) 147.

[32] W.Z. Li, Y. Yao, Q.M. Wang, Z.B. Bao, J. Gong, C. Sun, X. Jiang, J. Mater. Res., 23 (2008) 341.

[33] T.C. Rojas, S. El Mrabet, S. Domínguez-Meister, M. Brizuela, A. García-Luis, J.C. Sánchez-López, Surf. Coat. Technol. 211 (2012) 104.

Figure captions

Fig.1. AFM (a-b) and fracture cross-sectional SEM (d-f) morphologies of as-deposited CrNb10N (a, d), CrNb9Al4N (b, e) and CrNb8Al10N (c, f) coatings.

Fig.2. XRD patterns (a), grain size and lattice parameter (b) of the as-deposited coatings.

Fig.3. XRD patterns (a) of the coatings annealed at 800 ^{o}C and 900 ^{o}C, grain size and lattice parameter (b) of the 900 ^{o}C annealing coatings.

Fig.4. Hardness and Young's modulus of the coatings as-deposited, annealed at 900 ^{o}C for 1h.

Fig.5. Typical track morphologies of the CrNb10N (a, b), CrNb9Al4N (c, d) and CrNb8Al10N (e, f) coatings as-deposited (a, c, e) and annealed at 900^{o}C (b, d, f).

Fig.6. TGA curves (a) and XRD patterns (b) of selected coatings exposed to 1200 ^{o}C for 1h.

Fig.7. TGA curves (a), XRD patterns (b) and surface SEM images of the CrNb10N (c), CrNb9Al4N (d) and CrNb8Al10N (e) coatings after exposure at 800 ^{o}C/2h.

Fig.8. XRD patterns (a) and SEM images of the CrNb10N (b), CrNb9Al4N (c) and CrNb8Al10N (d) coatings after exposure at 900 ^{o}C/0.5h.

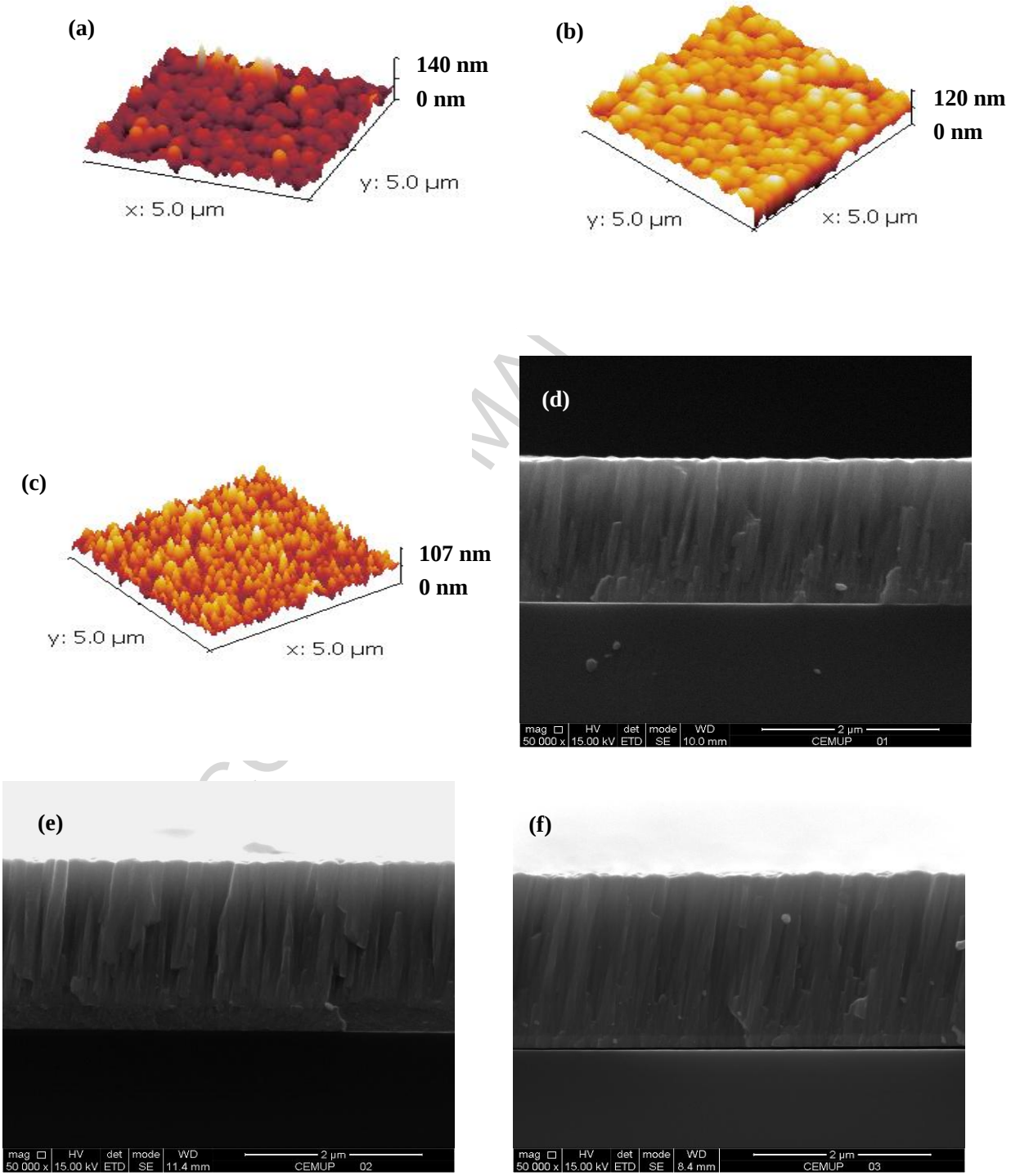

Fig.1. AFM (a-b) and fracture cross-sectional SEM (d-f) morphologies of as-deposited CrNb10N (a, d), CrNb9Al4N (b, e) and CrNb8Al10N (c, f) coatings.

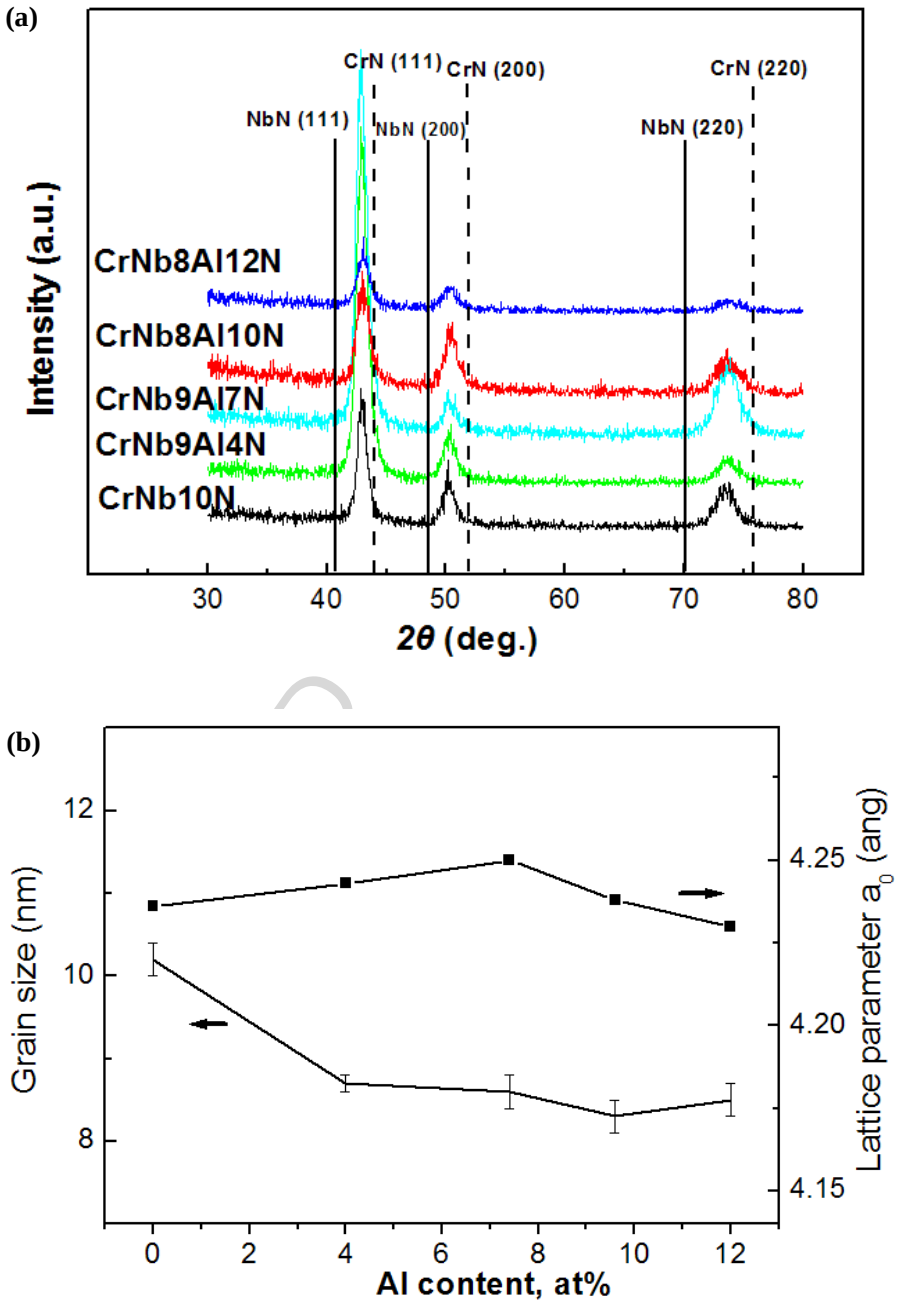

Fig.2. XRD patterns (a), grain size and lattice parameter (b) of the as-deposited coatings.

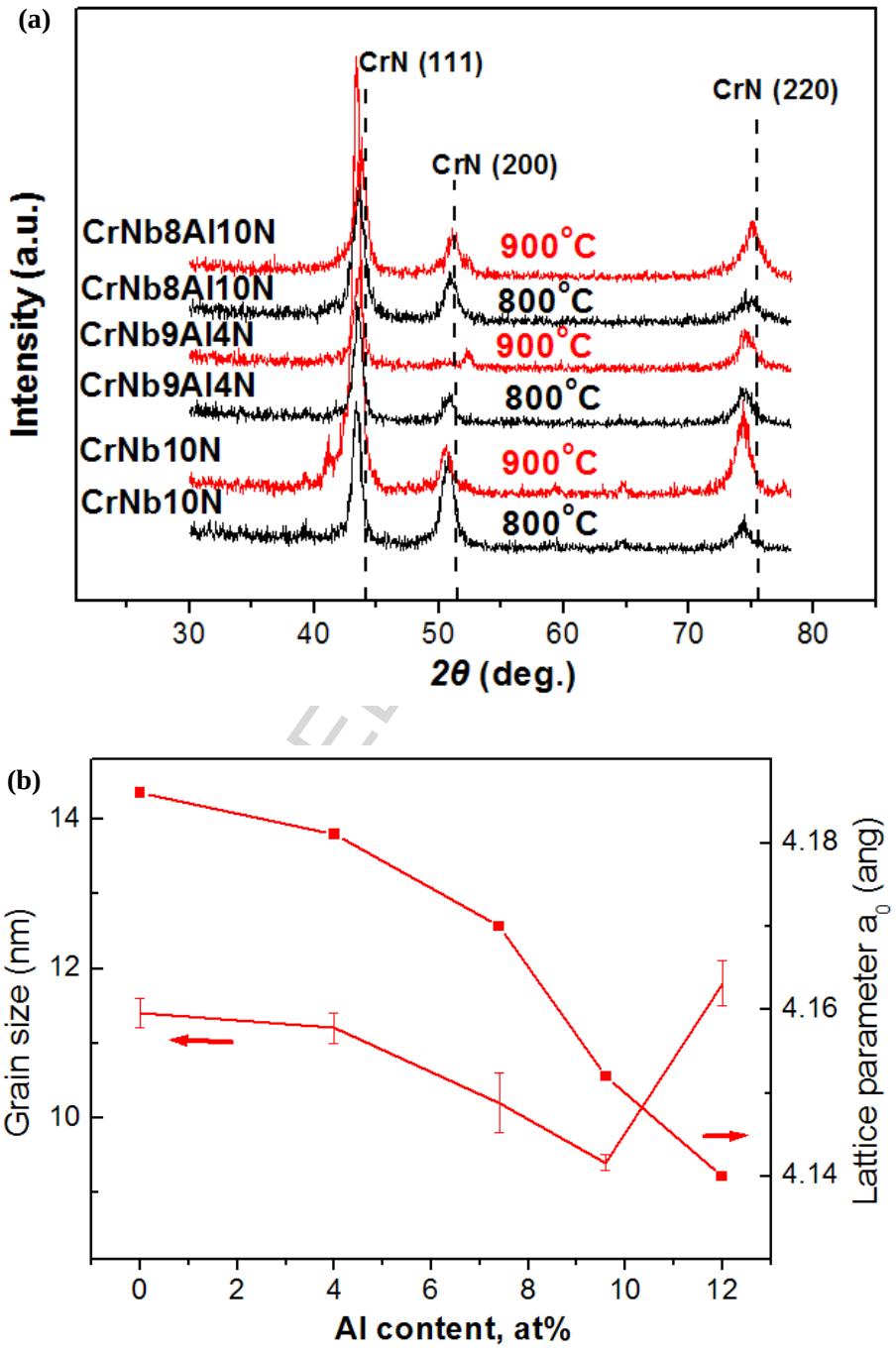

Fig.3. XRD patterns (a) of the coatings annealed at 800 ^{o}C and 900 ^{o}C, grain size and lattice parameter (b) of the 900 ^{o}C annealing coatings.

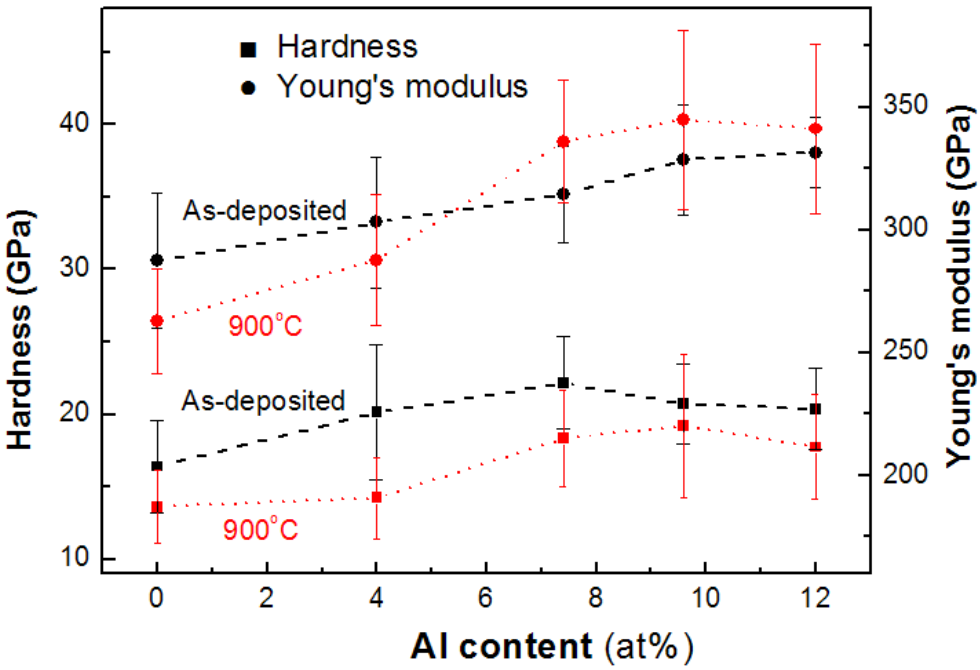

Fig.4. Hardness and Young's modulus of the coatings as-deposited, annealed at 900 ^{o}C for 1h.

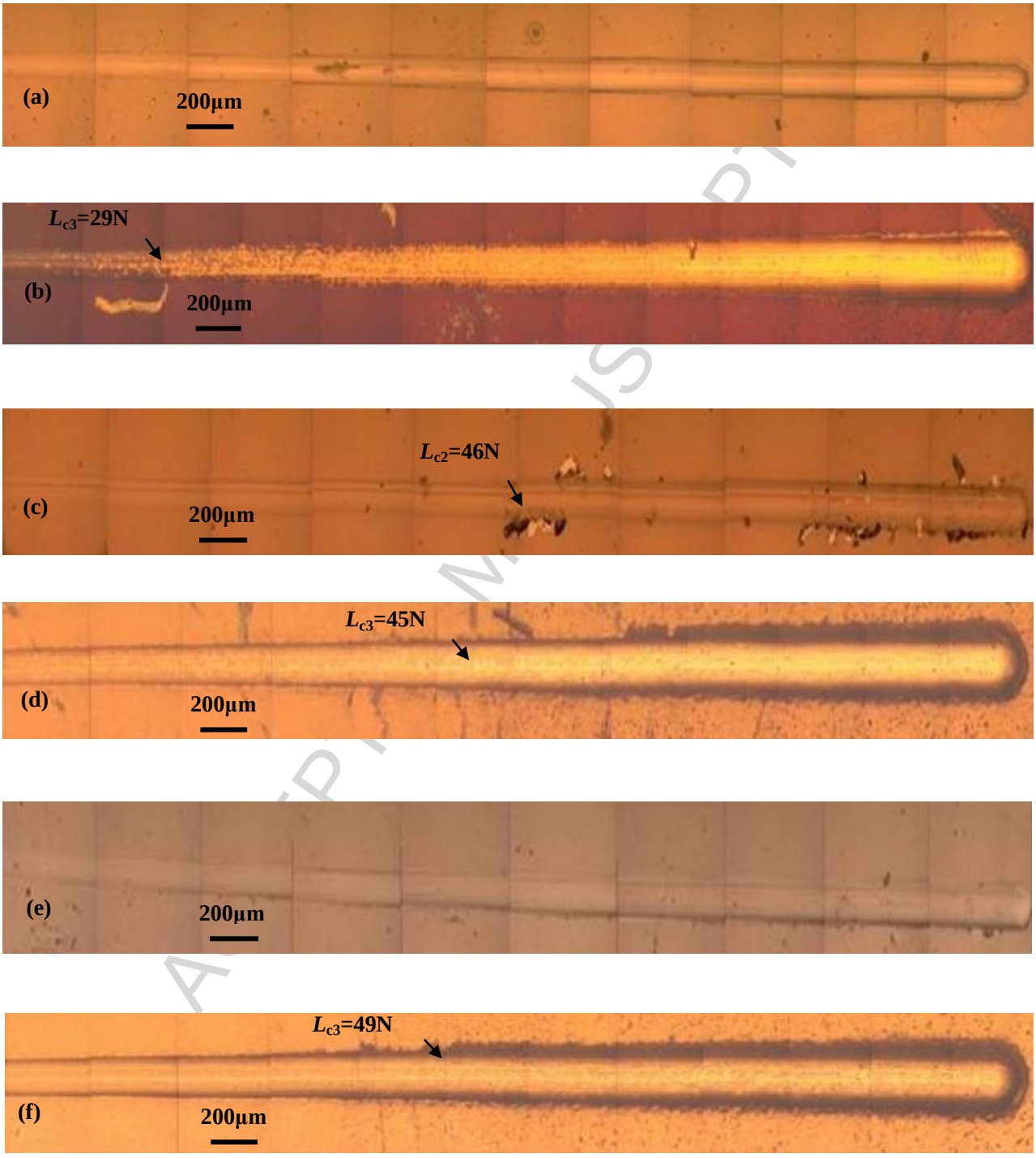

Fig.5. Typical track morphologies of the CrNb10N (a, b), CrNb9Al4N (c, d) and CrNb8Al10N (e, f) coatings as-deposited (a, c, e) and annealed at 900^{o}C (b, d, f).

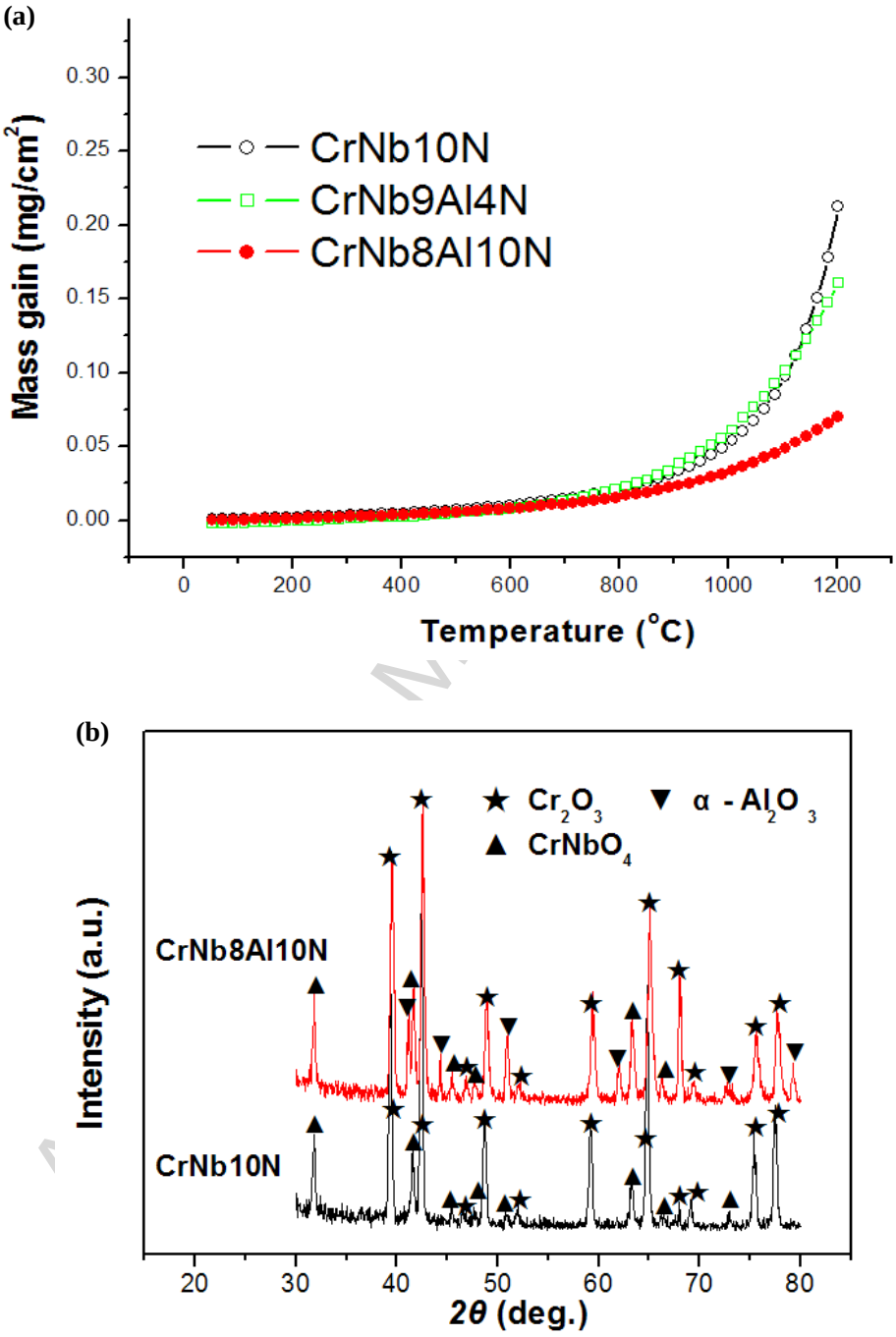

Fig.6. TGA curves (a) and XRD patterns (b) of selected coatings exposed to 1200 ^{o}C for 1h.

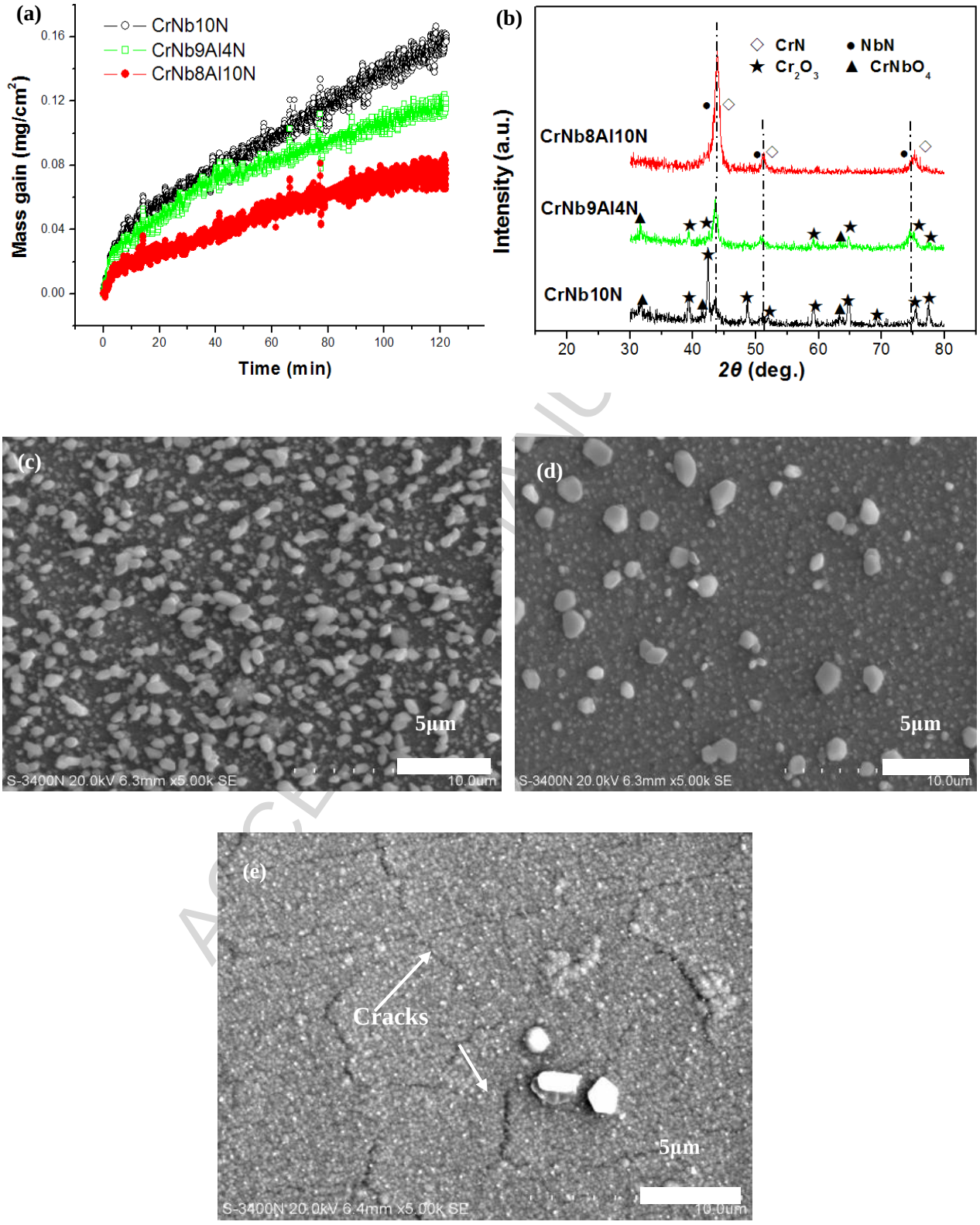

Fig.7. TGA curves (a), XRD patterns (b) and surface SEM images of the CrNb10N (c), CrNb9Al4N (d) and CrNb8Al10N (e) coatings after exposure at 800 ^{o}C/2h.

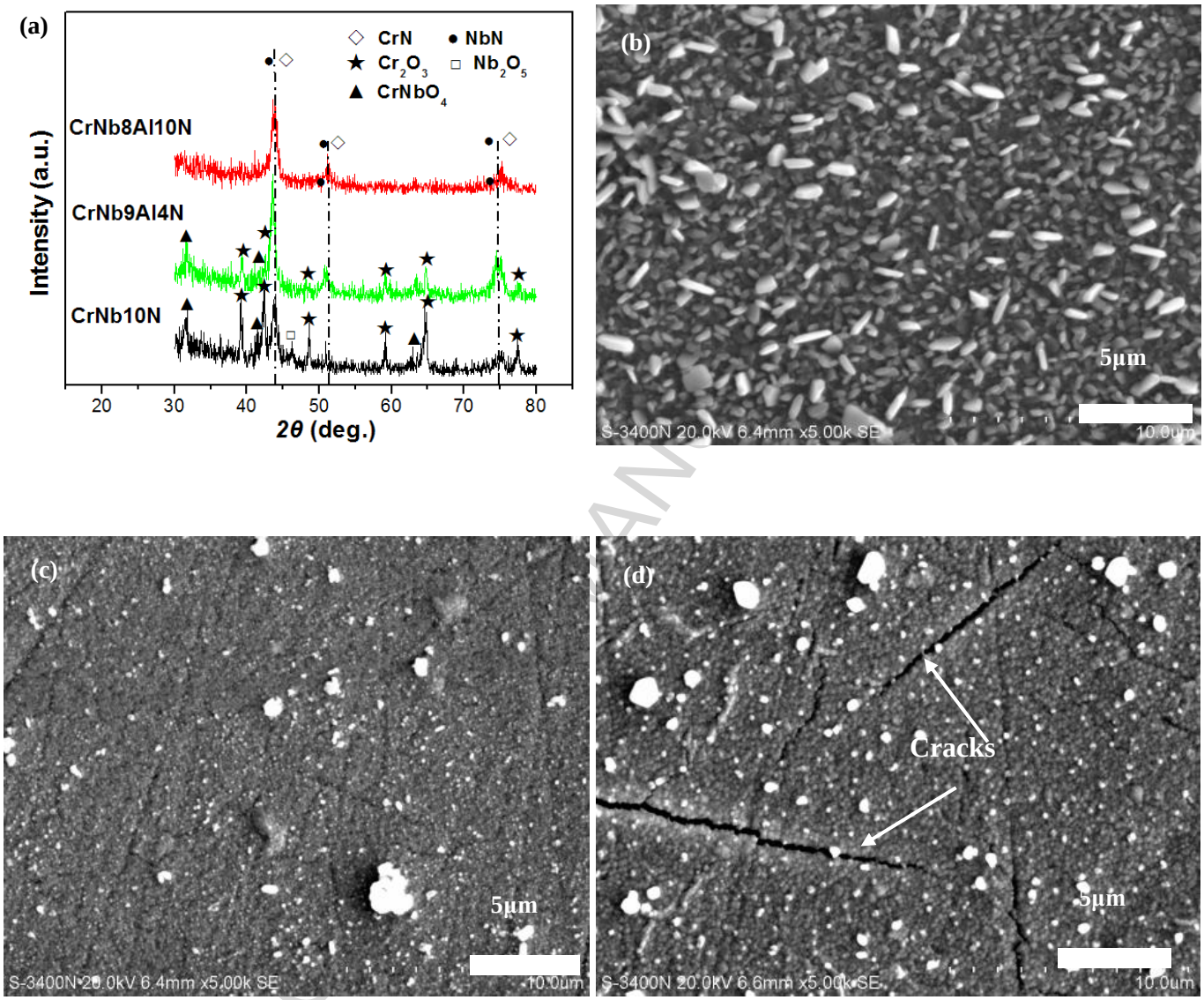

Fig.8. XRD patterns (a) and SEM images of the CrNb10N (b), CrNb9Al4N (c) and CrNb8Al10N (d) coatings after exposure at 900 ^{o}C/0.5h.

Table 1 Chemical composition, thickness, L_{c3} and designated name of the coatings.

Al Target Power Density (W/cm^2)	Chemical composition (at.%)*				Thickness (μm)	L_{c3} (N)		Designated name
	Nb	Cr	Al	N		as deposited	900°C annealing	
0.0	10.3	38.0	0.0	51.7	1.70	N/A	29	CrNb10N
0.75	9.2	34.8	4.0	52.0	1.80	N/A	45	CrNb9Al4N
1.5	8.5	33.1	7.4	51.0	1.85	N/A	48	CrNb9Al7N
2.25	7.9	29.7	9.6	52.8	1.95	N/A	49	CrNb8Al10N
3.0	7.6	28.2	12.0	52.2	2.05	N/A	36	CrNb8Al12N

* - all values ±0.2%

Highlights

- Al content is increased to 12 at.% as power density is 3 W/cm^2 in Al target.
- Cubic Cr(Nb)N and Cr(Nb, Al)N phases are thermally stable up to 900 ^{o}C.
- Onset oxidation temperature is close to 900 ^{o}C for all the Cr-Nb-Al-N coatings.
- High Al coatings exhibit stronger oxidation resistance.